Available online at www.sciencedirect.com
SCIENCE DIRECT®
Journal of Sound and Vibration 276 (2004) 1019–1041
JOURNAL OF SOUND AND VIBRATION
www.elsevier.com/locate/jsvi

# The influence of modal behaviour on the energy transmission between two coupled plates

W.S. Park, D.J. Thompson*, N.S. Ferguson

*Institute of Sound and Vibration Research, University of Southampton, Highfield, Southampton SO17 1BJ, UK*

Received 2 January 2003; accepted 14 August 2003

**Abstract**

The 'effective' coupling loss factor (CLF) of a particular realization of two coupled subsystems within a notional ensemble can differ from the ensemble average CLF. The variability in the effective CLF, or the transmission efficiency, due to the modal behaviour of the source and receiver subsystems has been examined for a system comprising two plates. A systematic investigation involving finite width semi-infinite plates and finite plates has been performed using a combination of wave models and dynamic stiffness approaches. By making both the source and receiver plates either finite or semi-infinite, it is shown that the modal behaviour of both the source and receiver plates affects the energy transmission between the two subsystems. Large variations in the energy transmission are found due to the modal behaviour of the finite receiver plate. The damping of the receiver plate controls the magnitude of these variations. However, variations in the energy transmission can also be attributed to the source subsystem modal characteristics, as seen for a finite source plate coupled to a semi-infinite receiver plate. It is shown that this variation is due to the predominance of particular angles of incidence at a given frequency. Damping of the source plate has only a small influence. For the present example, using a damping loss factor of 0.1, the influence of source and receiver modal behaviour is of a similar magnitude. For lower levels of damping the modal behaviour of the receiver subsystem becomes relatively more important.


## 1. Introduction

Since its beginnings over 40 years ago [1–3], Statistical Energy Analysis (SEA) has become quite widely used to solve high-frequency noise and vibration problems in vehicles, buildings and other structures [4–9]. The basic equation is the power balance equation [10]. Moreover, SEA is based on the concept of an ensemble. It provides an 'average' result for a set of notionally similar

*Corresponding author. Tel.: +44-23-8059-2510; fax: +44-23-8059-3190.
*E-mail address:* djt@isvr.soton.ac.uk (D.J. Thompson).

0022-460X/$ - see front matter 
doi:10.1016/j.jsv.2003.08.043

structures with properties drawn from a random set [8,11]. The various SEA parameters, notably the coupling loss factors (CLFs) that define the power flow between subsystems in terms of their energies, are defined as the averages for the ensemble. Fahy [8,11] discusses the impracticalities involved in measuring or predicting such ensemble averages for practical systems. Whilst this is not fully proved or resolved, SEA practitioners, instead, use estimates of the frequency-average response, on the assumption that this gives equivalent results. The frequency bandwidth has to be wide enough so that the underlying SEA assumptions relating the time-averaged power flow and the subsystem equilibrium energies are satisfied.

The successful application of SEA relies, therefore, amongst other things, on there being a large enough number of modes in each subsystem within each frequency band of interest [10]. This is equivalent to requiring that the acoustic or vibration field be diffuse [10]. It is also usually helpful if the modal overlap is sufficiently large, generally at least unity [12].

CLFs are often derived in terms of the wave transmission efficiencies at junctions between semi-infinite systems [13]. In this way the detail of the modes of individual systems are eliminated and smooth functions result. Other approaches have been adopted to allow for the effect of low modal overlap. Classically the CLFs are assumed to be independent of modal overlap, but at low modal overlap Mace et al. [14–16] and Yap and Woodhouse [17] have shown that the CLFs for an ensemble are dependent on modal overlap. For this situation, the results [14,16] show that the wave estimates substantially over-predict the coupling power and the CLF.

The power balance equations can equally be applied to an individual system, that is one member of the ensemble. In this case, the constants of proportionality between subsystem energy and power flow are no longer based on the ensemble average. In this paper the term *effective CLF* is used to refer to the CLF-like term appearing in the power balance equations for a single system realization. Such a system has distinct modal behaviour, as a result of which, the effective CLF may differ considerably from the ensemble average CLF. Putting this another way, the SEA ensemble prediction may differ considerably from the actual response of a given system.

Such deviations between the response of an individual realization and the ensemble average tend to be smaller at high frequencies. This is due to the fact that, for a constant damping loss factor, the modal overlap of most systems increases with increasing frequency. Additionally, the common use of octave or one-third octave bands means that the number of modes in a band becomes large at high frequencies. Conversely, at low frequencies the number of modes and the modal overlap can be low, and the deviations between the individual realization and the ensemble tend to be large.

Previous attempts to quantify the likely deviation between the behaviour of an individual realization and the ensemble average have been given by Lyon and DeJong [10] and Fahy and Mohammed [12]. Craik et al. [18] investigated the energy transmission at low frequencies in building structures composed of thick walls and floors and demonstrated that the variation in the point mobility of the *receiver* structure around its characteristic mobility was similar to the variation of the effective CLF around its ensemble average. This observation was used to derive an estimate for a confidence interval for the effective CLF. However, the question remains whether it is only modal behaviour of the receiver that is important.

The objective of this paper is to show to what extent modal behaviour of the source or receiver structure produces deviations in the effective CLF from the ensemble average CLF, due to the

presence of a non-diffuse field. In order to try to isolate the effects of source and receiver modal behaviour, models are considered in which the source and receiver are treated as finite or semi-infinite in turn. Throughout, as a particular case, the coupling between two rectangular flat plates joined along a common edge is considered. A combination of wave models and dynamic stiffness approaches is used. Two finite plates are analyzed first in Section 2 using a dynamic stiffness approach, to illustrate the effect of a non-diffuse field. A model of two semi-infinite plates of common finite width is then introduced in Section 3, to investigate the effect of the finite width compared with the usual results for plates of infinite width. Sections 4 and 5 consider a semi-infinite source plate coupled to a finite receiver and a finite source plate coupled to a semi-infinite receiver plate, respectively. By treating one or other plate as semi-infinite, its modal behaviour is eliminated, leaving only the modal behaviour of the other plate. Thus the extent to which these results deviate from those of two semi-infinite plates is a measure of the influence of the modal behaviour of each plate in turn.

## 2. Two coupled finite plates

Consider first two uniform rectangular plates of equal width $b$, and lengths $L_i$ coupled along a line that is simply supported and simply supported along the edges perpendicular to the joint, as shown in Fig. 1. Only flexural vibration is included. The response of this system can be calculated using a dynamic stiffness model for each plate [19,20].

The response amplitude $w_i$ of plate $i$ at frequency $\omega$ and position $(x, y)$ can be obtained from a summation over components with $n$ half-sine waves across the width $b$:

$$w_i(x, y) = \sum_{n=1}^{\infty} W_n(x) \sin\left(\frac{n\pi y}{b}\right), \tag{1}$$

where $W_n$ is the amplitude of the $n$th component ($i$ is omitted for clarity) and a time dependence of $e^{i\omega t}$ is assumed. This can be written in terms of the four free wave solutions for the plate

$$W_n(x, t) = \sum_{r=1}^{4} A_{nr} e^{k_{nr} x} \tag{2}$$

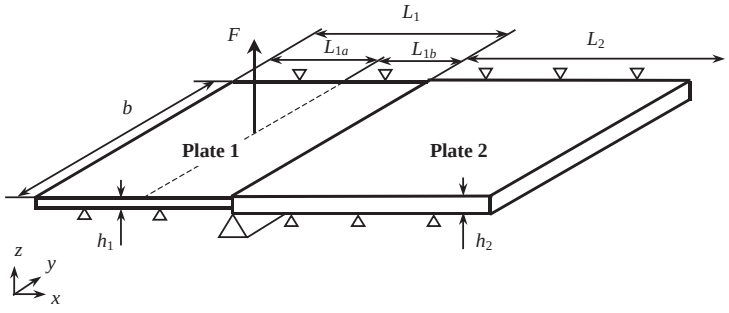


Fig. 1. Two rectangular plates joined at a simple support with a point force $F$ applied inside one plate.

with $A_{nr}$ the wave amplitudes and the four components of wavenumber in the $x$ direction given by

$$k_{nr} = \pm\sqrt{k_n^2 \pm k_f^2}, \tag{3}$$

where $k_n = n\pi/b$ is the component of wavenumber across the width and $k_f = (\rho h\omega^2/D)^{1/2}$ is the free flexural wavenumber in the plate, with $\rho h$ the mass per unit area and $D$ the bending stiffness. At low frequencies, $k_f < k_n$ and all the wavenumbers in Eq. (3) are real, so that only evanescent waves occur. When $k_f \geqslant k_n$, the wave of transverse order $n$ 'cuts on', that is two values of $k_{nr}$ become imaginary and propagating waves can exist. The frequency at which $k_f = k_n$ is referred to as the cut-on frequency and is given by

$$f_{cut-on} = \frac{\pi}{2}\left(\frac{n}{b}\right)^2\left(\frac{D}{\rho h}\right)^{1/2}. \tag{4}$$

From Eqs. (1) and (2), the displacement $w_i$, the rotation $\partial w_i/\partial x$, the bending moment $M$ and the shear force $S$ can each be written in terms of a sum over $n$ of the four wave amplitudes $A_{nr}$. For the $n$th component, by writing $\mathbf{A}_n^{\mathrm{T}} = \{A_{n1}A_{n2}A_{n3}A_{n4}\}$ and $\mathbf{u}_n^{\mathrm{T}} = \{W_n(0)W_n'(0)W_n(L)W_n'(L)\}$, it is found that

$$\mathbf{u}_n = \mathbf{p}_n\mathbf{A}_n, \tag{5}$$

where

$$\mathbf{p}_n = \begin{bmatrix} 1 & 1 & 1 & 1 \\ k_{n1} & k_{n2} & k_{n3} & k_{n4} \\ e_1 & e_2 & e_3 & e_4 \\ k_{n1}e_1 & k_{n2}e_2 & k_{n3}e_3 & k_{n4}e_4 \end{bmatrix} \tag{6}$$

where $e_i = \mathrm{e}^{k_{ni}L}$. Similarly, writing $\mathbf{F}_n^{\mathrm{T}} = \{-S_n(0)M_n(0)S_n(L) - M_n(L)\}$, it is found that

$$\mathbf{F}_n = \mathbf{q}_n\mathbf{A}_n, \tag{7}$$

where

$$\mathbf{q}_n = D\begin{bmatrix} k_{n1}^3 - (2-\mu)k_n^2k_{n1} & \cdots & k_{n4}^3 - (2-\mu)k_n^2k_{n4} \\ -k_{n1}^2 + \mu k_n^2 & \cdots & -k_{n4}^2 + \mu k_n^2 \\ -(k_{n1}^3 - (2-\mu)k_n^2k_{n1})e_1 & \cdots & -(k_{n4}^3 - (2-\mu)k_n^2k_{n4})e_4 \\ (k_{n1}^2 - \mu k_n^2)e_1 & \cdots & (k_{n4}^2 - \mu k_n^2)e_4 \end{bmatrix} \tag{8}$$

with $\mu$ the Poisson ratio. The wave amplitudes $\mathbf{A}_n$ can be eliminated from Eqs. (5) and (7) to give the dynamic stiffness matrix for flexural vibrations of transverse order $n$:

$$\mathbf{K}_n = \mathbf{q}_n\mathbf{p}_n^{-1}. \tag{9}$$

The two coupled plates of Fig. 1, with a point force at a location within the left-hand plate, can be modelled using three dynamic stiffness elements, one either side of the force on the source plate and the other representing the receiver plate. These elements are assembled in the usual way, reduced by applying appropriate boundary conditions and then solved to obtain the response. The outer edges are considered to be free. The point force is Fourier-decomposed into components for each $n$ and the response at each edge (node) for each $n$ is obtained by inverting the

reduced dynamic stiffness matrix. Then the wave amplitudes in each plate element can be found from Eq. (5) and the response at a general interior position from Eq. (2).

Single point excitation is applied at a large number of randomly chosen points, avoiding positions close to the edges. In order to simulate a 'rain-on-the-roof' type excitation, a total of 400 excitation points are used on each plate, which has been shown in a previous investigation to be sufficient to obtain a reasonable estimate for the CLF reducing variations due to the particular points chosen to less than 0.1 dB [19].

Each point force excites vibration in many different transverse orders, $n$, across the plate width. For a given frequency, all such components whose cut-on frequency is below the frequency under consideration need to be included. By exciting first one plate and then the other, in each case averaging over 400 excitation points, a numerical simulation equivalent to the experimental Power Injection Method [21] is performed. The response is numerically integrated to give accurate predictions of the total strain energy in each plate, $E_i$. These are calculated for each transverse order $n$ and then summed. This allows the 'effective' CLFs, $\hat{\eta}_{ij}$, to be determined from

$$\begin{Bmatrix} \hat{\eta}_{12} \\ \hat{\eta}_{21} \end{Bmatrix} = \frac{1}{\omega} \begin{bmatrix} E_1^{(1)} & -E_2^{(1)} \\ -E_1^{(2)} & E_2^{(2)} \end{bmatrix}^{-1} \begin{Bmatrix} \omega\eta_2 E_2^{(1)} \\ \omega\eta_1 E_1^{(2)} \end{Bmatrix}, \tag{10}$$

where $E_1$ and $E_2$ are the total time-averaged energies, the superscript, (1) or (2), means the excitation is applied to subsystem 1 or 2, and $\eta_i$ is the damping loss factor of subsystem $i$. It is assumed that $\eta_{ij}^{(1)} = \eta_{ij}^{(2)}$, i.e., that the CLFs are independent of which subsystem is being excited.

The effective CLFs for two coupled aluminium plates, calculated using Eq. (10), are shown in Fig. 2. These have width $b = 1.0$ m, lengths $L_1 = 0.5$ m, $L_2 = 1.0$ m, thicknesses $h_1 = 3.0$ mm, $h_2 = 2.0$ mm, Young's modulus $E = 7.24 \times 10^{10}$ N/m$^2$, the Poisson ratio $\mu = 0.333$ and material density $\rho = 2794$ kg/m$^3$. The damping loss factor $\eta_1 = \eta_2 = 0.1$. Although this is rather high for material damping, it is chosen as more typical of a built-up structure and in particular to avoid a situation of strong coupling where $\eta \ll \eta_{ij}$. Also shown are the results for two infinite plates $\eta_{ij\infty}$, determined from the diffuse field transmission coefficient $\tau_{ij,d}$. From Ref. [13] this can be written as

$$\eta_{ij\infty} = \frac{c_{gi} b \tau_{ij,d}}{\pi \omega S_i}, \tag{11}$$

where $c_{gi}$ is the group velocity of the source subsystem $i$, $b$ is the junction length, $S_i$ is the surface area of the source subsystem and $\omega$ is the circular frequency (rad/s). A correction factor is applied here to account for the relationship between $\tau_{ij,d}$ and $\eta_{ij\infty}$ when there is high transmission [22], i.e.,

$$\eta_{ij\infty} = \frac{c_{gi} b}{\pi \omega S_i} \frac{2\tau_{ij,d}}{(2 - \tau_{ij,d})}. \tag{12}$$

The calculated effective CLFs agree well with the semi-infinite result $\eta_{ij\infty}$ at high frequencies. At low frequencies, the predicted CLFs fluctuate considerably relative to $\eta_{ij\infty}$, with differences of up to a factor of 10 (10 dB). The first mode of plate 1 is at 12 Hz and that of plate 2 at 6 Hz, so below these frequencies it would not be expected to be appropriate to use an SEA formulation. The modal overlap becomes equal to unity at about 200 Hz for plate 1 and 60 Hz for plate 2. As shown in Refs. [12,19] variations in CLF are considerably greater when the modal overlap is less than unity.

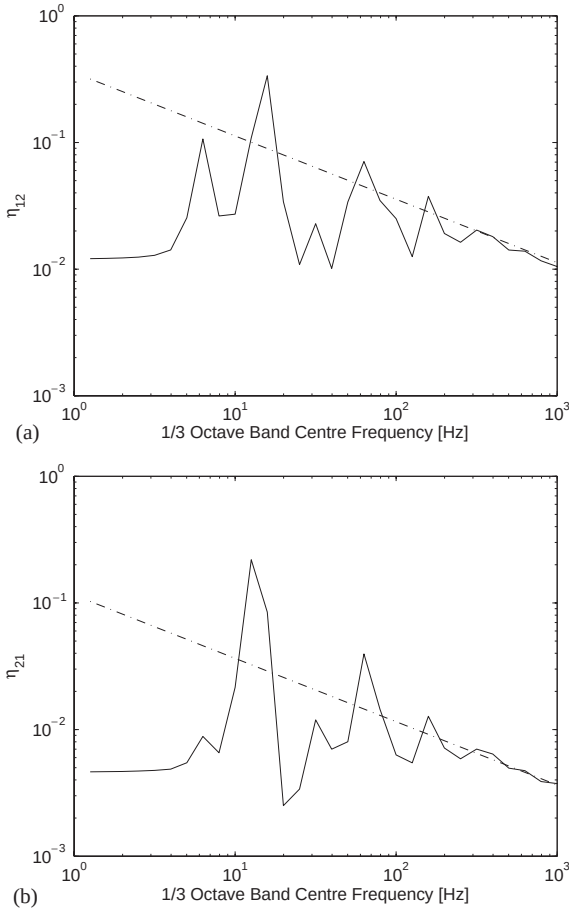


Fig. 2. Comparison of CLFs: (a) $\hat{\eta}_{12}$; (b) $\hat{\eta}_{21}$ obtained from ——, 'numerical experiment' on two finite plates; - · - · -, semi-infinite plates.

## 3. Two semi-infinite plates of finite width

Two coupled semi-infinite thin plates of finite width $b$ are next considered in order to study the restriction imposed by a finite width. The two plates are assumed to be simply supported along their longitudinal edges, $y = 0$ and $b$, and joined at the interface $x = 0$, as shown in Fig. 3. At $x = 0$ a simple support is also assumed, as above. In this model, it is assumed that there is no damping in the two semi-infinite plates.

Allowable wave solutions have a trace wavenumber in the $y$ direction $k_n = n\pi/b$ for positive integer values of $n$. Considering only flexural waves, the motion of plate 1 of order $n$ has the form

$$w_1(x, y) = (A_{in}\mathrm{e}^{-k_{11}x} + A_r\mathrm{e}^{k_{11}x} + A_{nr}\mathrm{e}^{k_{21}x})\sin(k_n y), \tag{13}$$

where $A_{in}, A_r$ and $A_{nr}$ are the complex amplitudes of the propagating incident and reflected and non-propagating nearfield waves at the interface, and $k_{11}$ and $k_{21}$ are the respective propagating

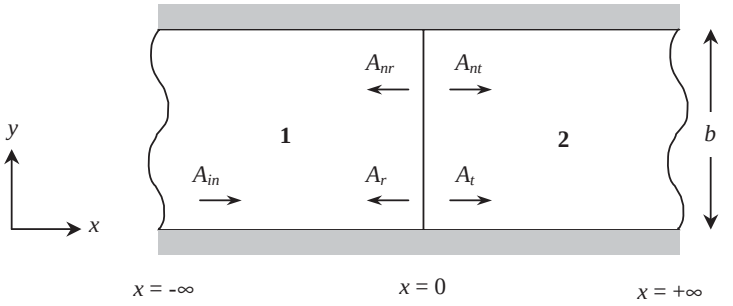


Fig. 3. Two semi-infinite plates of finite width $b$ joined at a line $x = 0$ which is simply supported.

and nearfield wavenumbers of plate 1. These wavenumbers are the roots obtained from the wave equation for plate 1, i.e.,

$$k_{11} = (k_n^2 - k_{f1}^2)^{1/2}, \quad k_{21} = (k_n^2 + k_{f1}^2)^{1/2}, \tag{14}$$

where $k_{f1} = (\rho_1 h_1 \omega^2 / D_1)^{1/4}$ is the free bending wavenumber of plate 1 as before. The effective angle of incidence $\theta$ at the interface $x = 0$ can be obtained from

$$\theta = \tan^{-1}\left|\frac{k_n}{k_{11}}\right|, \tag{15}$$

where $\theta = 0$ corresponds to normal incidence.

Similarly for plate 2, the out-of-plane displacement of order $n$ is

$$w_2(x, y) = (A_t e^{-k_{12}x} + A_{nt} e^{-k_{22}x}) \sin(k_n y), \tag{16}$$

where $A_t$ and $A_{nt}$ are the complex amplitudes of the propagating transmitted and non-propagating nearfield waves at the interface, and $k_{12}$ and $k_{22}$ are the corresponding wavenumbers of plate 2. These wavenumbers are the roots obtained from the wave equation for plate 2, similar to Eq. (14).

Constraining the displacement along the joint, only rotational motion is allowed. Applying the continuity and equilibrium conditions at the joint, one can determine the amplitude of each wave.

Substituting Eqs. (13) and (16) into these boundary conditions, the four unknown amplitudes can be determined in terms of the amplitude of the incident wave $A_{in}$, as follows:

$$\mathbf{B}_1 \mathbf{A}_1 = \mathbf{C}_1, \tag{17}$$

where

$$\mathbf{B}_1 = \begin{bmatrix} 1 & 1 & 0 & 0 \\ 0 & 0 & 1 & 1 \\ k_{11} & k_{21} & k_{12} & k_{22} \\ D_1 k_{11}^2 & D_1 k_{21}^2 & -D_2 k_{12}^2 & -D_2 k_{22}^2 \end{bmatrix}, \tag{18}$$

$$\mathbf{A}_1 = \begin{bmatrix} \frac{A_r}{A_{in}} & \frac{A_{nr}}{A_{in}} & \frac{A_t}{A_{in}} & \frac{A_{nt}}{A_{in}} \end{bmatrix}^{\mathrm{T}} \quad \text{and} \quad \mathbf{C}_1 = [-1 \quad 0 \quad k_{11} \quad -D_1 k_{11}^2]^{\mathrm{T}}, \tag{19}$$

which can be solved by inversion of $\mathbf{B}_1$.

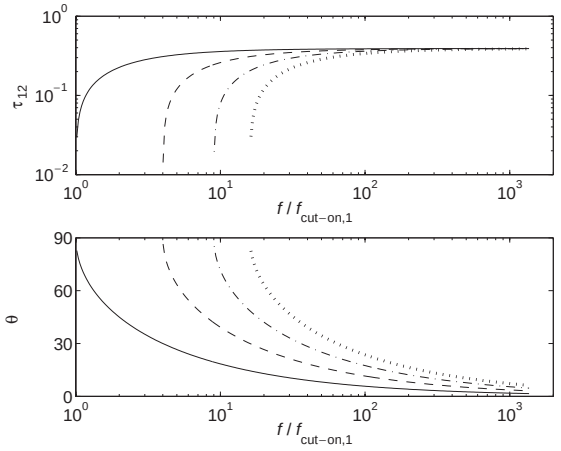


Fig. 4. Transmission efficiencies and the angle of incidence predicted for two semi-infinite aluminium plates of width $b = 1$ m, thickness of the source plate $h_1 = 3$ mm, and thickness of the receiver plate $h_2 = 2$ mm. Four curves represent the results for different transverse orders $n$: ——, $n = 1$; - - - -, $n = 2$; - · - · -, $n = 3$; ·····, $n = 4$. The $x$-axis is a non-dimensional frequency, $f/f_{cut\text{-}on,1}$, where $f_{cut\text{-}on,1}$ is the cut-on frequency of the source plate for $n = 1$ ($f_{cut\text{-}on,1} = 7.34$ Hz).

Above the cut-on frequency for order $n$, power is transmitted by the propagating waves. The nearfield waves do not transmit any energy at any frequency. In general, the transmitted powers are proportional to the propagating wave amplitude squared, but also depend on the plate properties. As the incident and reflected waves exist in the same plate, the transmission efficiency $\tau$ can be obtained most easily from

$$\tau = 1 - \left|\frac{A_r}{A_{in}}\right|^2. \tag{20}$$

Fig. 4 shows example results for a source plate of thickness 3 mm and a receiver plate of thickness 2 mm, both of aluminium with no damping. The transmission efficiency only exists above the cut-on frequency of both plates for any particular value of $n$. Below the cut-on frequency of plate 1 (here 7.34 Hz), no propagating incident wave will occur and it is meaningless to calculate the transmission efficiency. Below the cut-on frequency in the receiver plate (here 4.89 Hz), no energy will be transmitted into pure propagating waves in the receiver plate and the transmission efficiency is zero. Thus the transmission efficiencies are zero up to the higher of the two cut-on frequencies, which in this case is for plate 1. Then they rise gradually and at high frequencies they tend to the result for normal incidence for semi-infinite plates, in this case 0.39 for these thicknesses (3 and 2 mm). This can be explained by consideration of the angle of incidence, given in Eq. (15). At cut-on, $k_n = k_f$ and wave propagation occurs in a direction parallel to the joint, i.e., $k_{11} = 0$, whereas at high frequencies $k_n/k_{11} \to 0$ and $\theta \to 0$. Note that the cut-on frequency for transverse order $n$ is $n^2 f_{cut\text{-}on,1}$; i.e., $f_{cut\text{-}on,2} = 4f_{cut\text{-}on,1}, f_{cut\text{-}on,3} = 9f_{cut\text{-}on,1}$, etc.

For two semi-infinite plates the transmission efficiency for oblique incidence is given in Ref. [13]. For the case of grazing incidence $\theta = \pm\pi/2$, $\tau_{12}$ is zero. As the frequency increases, the direction of propagation gradually approaches normal, $\theta \to 0$ and $\tau_{12}$, for a given $n$, tends to $\tau_{12}(0)$, which is 0.39 for these values of plate thickness. As more orders across the plate width, $n$, cut on

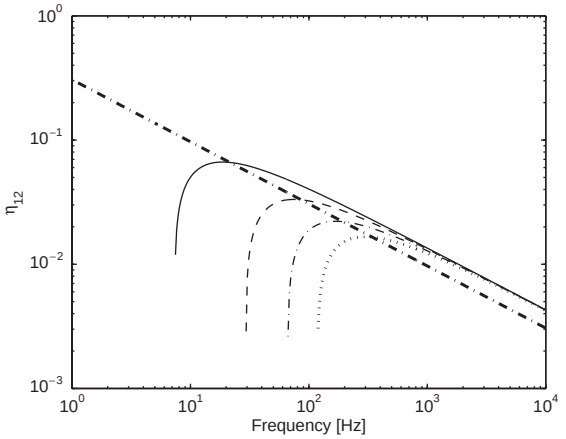


Fig. 5. CLFs derived from models of two infinite aluminium plates (thickness of the source plate $h_1 = 3$ mm and thickness of the receiver plate $h_2 = 2$ mm) and of two semi-infinite aluminium plates of finite width $b = 1$ m: ——, $n = 1$; - - - -, $n = 2$; - · - · -, $n = 3$; ·····, $n = 4$. Thick dash dot line represents the CLF result for two semi-infinite plates $\eta_{12\infty}$.

and are included in the incident field, this approximates more closely to a diffuse field, with the incident energy not primarily being at a single angle of incidence. Thus, the sum over all such $n$ will tend to the diffuse field value of $\tau_{12,d}$ found for infinite plates.

Although the CLF is only defined for finite plates, the transmission efficiency, $\tau$, for two semi-infinite plates can be used to estimate the CLF of an equivalent finite plate by using Eq. (11). The CLF results, using these semi-infinite plate transmission efficiencies for particular transverse orders, are shown in Fig. 5 for a source plate of area $0.5\,\mathrm{m}^2$. Individual CLFs for particular orders converge to the normal incidence result, which are individually greater than the infinite plate diffuse result $\eta_{12\infty}$.

## 4. A semi-infinite plate of finite width coupled to a finite plate

### 4.1. Model

In this section, a model is considered in which a semi-infinite source plate is connected to a finite receiver plate of length $L_2$, as shown in Fig. 6. The right-hand edge of plate 2 is assumed to be free to correspond to the finite plates considered in Section 2. This model is used to investigate the influence of the modal behaviour of the receiver plate on the energy transmission. An incident wave $A_{in}$ is introduced in the semi-infinite source plate, as in Section 3. The transmission efficiencies are evaluated for different thickness ratios of the source plate to the receiver plate and the results are then considered in terms of the modal behaviour of the finite receiver plate.

The out-of-plane displacement of plate 2, given in Eq. (16), must be extended to include a second reflected wave and a second nearfield wave.

$$w_2(x,y) = (A_t e^{-k_{12}x} + A_{nt} e^{-k_{22}x} + A_{r2} e^{k_{12}x} + A_{nr2} e^{k_{22}x}) \sin(k_n y), \tag{21}$$

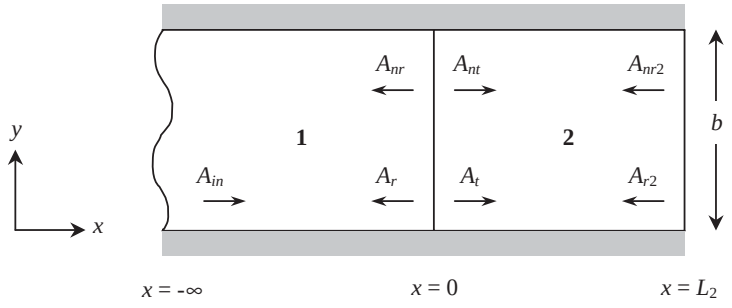


Fig. 6. Semi-infinite (source) plate of finite width $b$ connected to a finite (receiver) plate.

where $A_{r2}$ and $A_{nr2}$ are the complex amplitudes of the reflected propagating and non-propagating nearfield waves from the right-hand edge of plate 2. Applying the equilibrium and continuity conditions at the joint and boundary conditions at the right-hand free edge of plate 2 to this equation and Eq. (1), the six unknown amplitudes can be solved in terms of $A_{in}$. The additional boundary conditions are that the bending moment and the shear force at the right-hand edge of plate 2 are equal to zero.

Substituting Eqs. (13) and (21) into these boundary conditions gives

$$\mathbf{B}_2\mathbf{A}_2 = \mathbf{C}_2, \tag{22}$$

where

$$\mathbf{B}_2 = \begin{bmatrix} 1 & 1 & 0 & 0 & 0 & 0 \\ 0 & 0 & 1 & 1 & 1 & 1 \\ k_{11} & k_{21} & k_{12} & k_{22} & -k_{12} & -k_{22} \\ D_1k_{11}^2 & D_1k_{21}^2 & -D_2k_{12}^2 & -D_2k_{22}^2 & -D_2k_{12}^2 & -D_2k_{22}^2 \\ 0 & 0 & b_{12}e_{12}^- & b_{22}e_{22}^- & b_{12}e_{12}^+ & b_{22}e_{22}^+ \\ 0 & 0 & c_{12}e_{12}^- & c_{22}e_{22}^- & -c_{12}e_{12}^+ & -c_{22}e_{22}^+ \end{bmatrix}, \tag{23}$$

in which $b_{ij} = k_{ij}^2 - \mu_j k_n^2$, $\quad c_{ij} = k_{ij}\{-k_{ij}^2 + (2-\mu_j)k_n^2\}$, $\quad e_{ij}^+ = \mathrm{e}^{k_{ij}L_j}$, $\quad e_{ij}^- = \mathrm{e}^{-k_{ij}L_j}$,

$$\boldsymbol{A}_2 = \left[\frac{A_r}{A_{in}} \quad \frac{A_{nr}}{A_{in}} \quad \frac{A_t}{A_{in}} \quad \frac{A_{nt}}{A_{in}} \quad \frac{A_{r2}}{A_{in}} \quad \frac{A_{nr2}}{A_{in}}\right]^{\mathrm{T}} \tag{24}$$

and

$$\mathbf{C}_2 = \begin{bmatrix} -1 & 0 & -k_{11} & -D_1k_{11}^2 & 0 & 0 \end{bmatrix}^{\mathrm{T}}. \tag{25}$$

The transmission efficiency $\tau$ of the joint between the two plates can be obtained from Eq. (20).

Fig. 7(a) shows results for an example case corresponding to the geometry of Fig. 1; here a semi-infinite source plate of thickness 3 mm, finite width 1 m is coupled to a damped finite receiver plate of thickness 2 mm, length 1 m, each of aluminium. Results are given for $n = 1$. At low frequencies, the transmission efficiency oscillates considerably around that for two semi-infinite plates, whereas it converges to that for two semi-infinite plates ($\tau_{12} = 0.42$) as frequency increases. It is noted that the transmission efficiency for two semi-infinite plates here differs from that shown

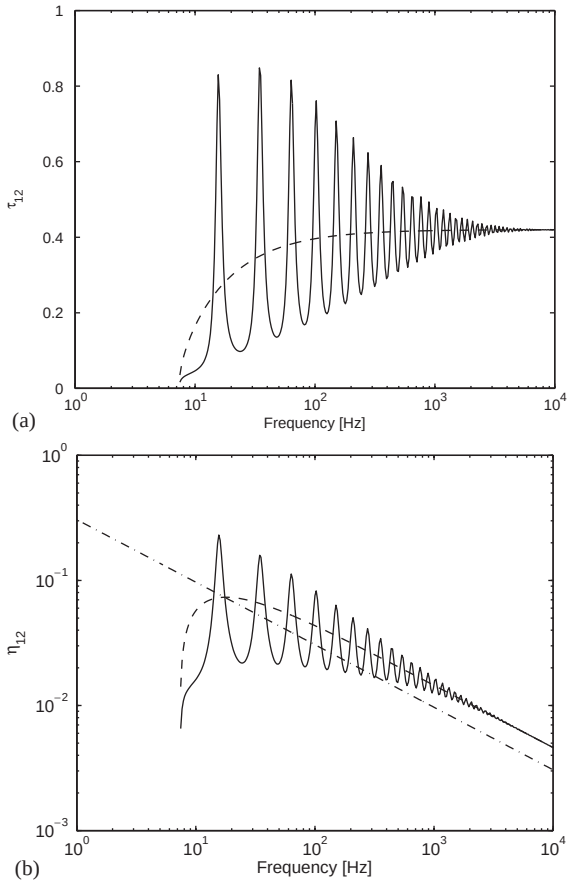


Fig. 7. (a) Transmission efficiency $\tau_{12}$ for a semi-infinite plate (thickness $h_1 = 3\,\text{mm}$, $\eta_1 = 0$) of finite width ($b = 1\,\text{m}$) coupled to a finite plate (thickness $h_2 = 2\,\text{mm}$, length $L_2 = 1\,\text{m}$, $\eta_2 = 0.1$) for $n = 1$: ——, semi-infinite to finite plates; - - - -, two semi-infinite plates of finite width; (b) CLF obtained from $\tau_{12}$ for source plate of length 0.5 m for $n = 1$; ——, semi-infinite to finite plates; - - - -, two semi-infinite plates of finite width; -·-·-, two semi-infinite plates (diffuse incidence).

in Fig. 4, $\tau_{12}(0) = 0.39$. In the present case, it is assumed that there is no damping in the semi-infinite source plate ($\eta_1 = 0$), as before, but the receiver plate is damped with a loss factor $\eta_2 = 0.1$. This loss factor makes the bending wavenumber complex and affects the transmission efficiency. The influence of the damping of the receiver plate is investigated in more detail in the following section. The peaks and troughs in the transmission efficiency for the finite receiver plate are related to the modal behaviour of the receiver plate. This is discussed further in Section 4.3.

Fig. 7(b) shows the CLF results for a transverse order $n = 1$ estimated from the above transmission efficiency by Eq. (11). The infinite plate diffuse result $\eta_{12\infty}$ is also shown. In converting the result to a CLF, the length of the source plate is taken as 0.5 m. The CLF for the finite receiver plate for $n = 1$ converges to the normal incidence result as frequency increases and these CLFs are greater than the infinite plate diffuse result $\eta_{12\infty}$. When the transmission efficiencies are averaged for all possible transverse orders $n$, the CLF for the finite receiver plate

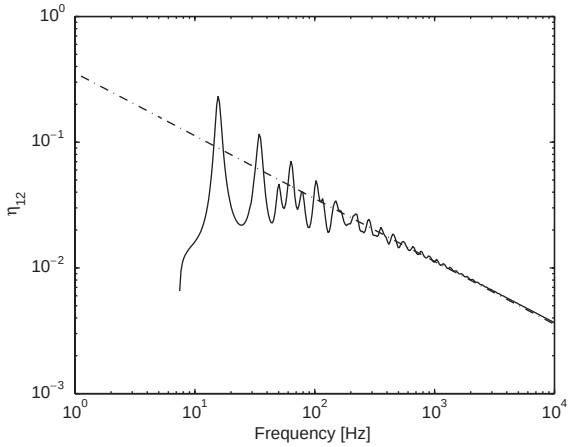


Fig. 8. The CLF for the finite receiver plate with $b = 1\,\text{m}$, $L_2 = 1\,\text{m}$, $h_2 = 2\,\text{mm}$; ——, the average result for all possible transverse orders $n$; - · · · -, the CLF for two semi-infinite plates.

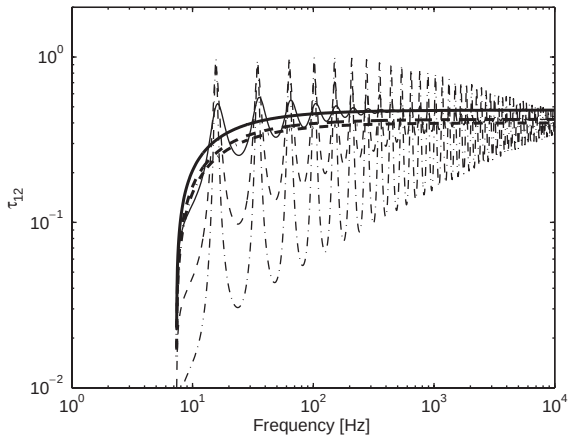


Fig. 9. The influence of receiver damping on the transmission efficiency for a semi-infinite plate (thickness $h_1 = 3\,\text{mm}$) of finite width ($b = 1\,\text{m}$) coupled to a finite plate (thickness $h_2 = 2\,\text{mm}$, length $L_2 = 1\,\text{m}$) for $n = 1$: ——, $\eta_2 = 0.3$; - - - -, $\eta_2 = 0.1$; - · · · -, $\eta_2 = 0.03$. Thick lines represent the corresponding results for the two-semi infinite plates with damping in the receiver plate.

converges to $\eta_{12\infty}$, at high frequency as shown in Fig. 8. Here $\eta_{12\infty}$ includes the factor $2/(2-\tau)$ as in Eq. (12). It will be recalled that the modal overlap for the receiver plate is less than unity for frequencies above 60 Hz. At this frequency, the result in Fig. 8 deviates by up to $\pm 3\,\text{dB}$ from the semi-infinite result. Even at 300 Hz the deviations are around $\pm 1\,\text{dB}$.

### 4.2. The influence of damping of the receiver plate

The influence of damping in the receiver plate was investigated for three damping values, $\eta_2 = 0.03$, 0.1 and 0.3, and the transmission efficiencies are shown in Fig. 9. As the damping of the receiver plate increases, this plate dissipates more power so that less power is reflected back

towards the joint. As a result of this, the transmission efficiency $\tau_{12}$ oscillates less with frequency and converges more quickly to that for two semi-infinite plates with the appropriate receiver damping. The high-frequency asymptotes of the transmission efficiencies converge to that for the undamped semi-infinite receiver plate, as damping of the receiver plate decreases, i.e., $\tau_{12} = 0.48$, 0.42 and 0.40 for $\eta_2 = 0.3$, 0.1 and 0.03, respectively, compared with 0.39 for the undamped case. However, if there were no damping in the finite receiver plate, all the power flowing into the receiver plate would be reflected out of it again and $\tau$ would be zero.

### 4.3. The influence of the modal behaviour of the finite receiver plate

The transmission efficiencies depend on the ratio of the thicknesses of the source and receiver plates. Fig. 10 shows the transmission efficiencies for both finite and infinite receiver plates of thickness 2 mm connected to an infinite source plate of thickness 0.67, 2 and 6 mm. There is no damping in the source plate whilst the receiver plate is damped with $\eta_2 = 0.1$ in each case.

The transmission efficiency tends to a maximum asymptotic value when the thicknesses of the two plates are equal and this asymptote reduces when the ratio of thicknesses is large or small. At high frequencies, the transmission efficiency for the finite receiver plate converges to that for two semi-infinite plates allowing for damping in the receiver plate.

The frequencies of the peaks vary only slightly as the thickness of the source plate varies, whereas if the thickness of the receiver plate is changed this affects the peak frequencies according to the modal behaviour of the receiver plate. In order to compare these results with the modal behaviour, the natural frequencies of the uncoupled receiver plate have been calculated for two sets of boundary conditions on the edge usually coupled to the infinite plate (simply supported or clamped). The peaks in the transmission efficiency are found to occur between the natural frequencies of the uncoupled receiver finite plate with either simply supported or clamped

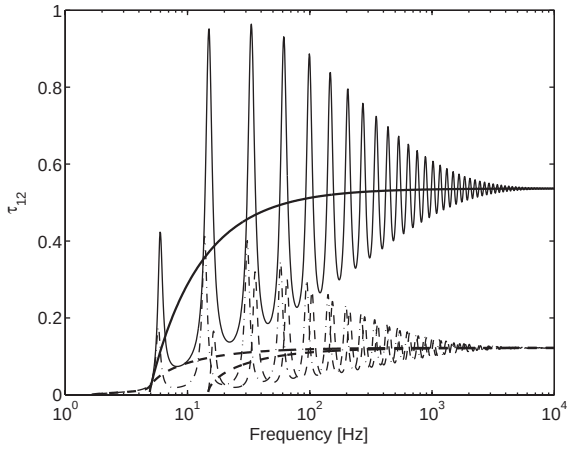


Fig. 10. Transmission efficiencies for a semi-infinite source plate connected to a finite plate (width $b = 1$ m, length $L_2 = 1$ m, thickness $h_2 = 2$ mm, DLF $\eta_2 = 0.1, n = 1$) for different values of $h_1$: ----, $h_1 = 6$ mm; ——, $h_1 = 2$ mm; -·-·-, $h_1 = 0.7$ mm. Also shown are the corresponding results for two semi-infinite plates of finite width, which are the asymptotes for the former results.

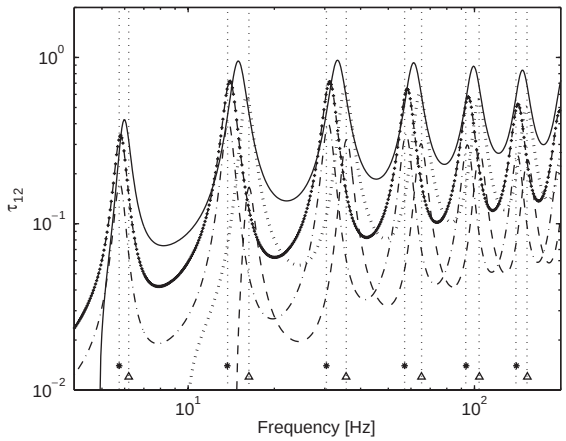


Fig. 11. Transmission efficiencies for an infinite source plate coupled to a finite receiver plate ($b = 1\,\text{m}$, $L_2 = 1\,\text{m}$, $h_2 = 2\,\text{mm}$, $n = 1$), for different values of $h_1$; - - - -, $h_1 = 6\,\text{mm}$; ·····, $h_1 = 4\,\text{mm}$; ——, $h_1 = 2\,\text{mm}$; –+–+–, $h_1 = 1\,\text{mm}$; - · - · -, $h_1 = 0.7\,\text{mm}$: natural frequencies of finite plate; ∗, F–S–S–S; △, F–S–C–S. The vertical dotted lines show the natural frequency of each mode.

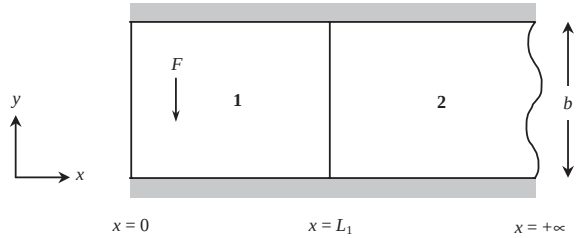


Fig. 12. Finite (source) plate connected to a semi-infinite (receiver) plate of finite width $b$.

boundary condition at the interface, i.e., F–S–S–S or F–S–C–S, as shown in Fig. 11 for various values of source plate thickness. At resonances of the finite receiver plate, its wave impedance is low, producing a maximum in the transmitted energy, and hence in the power dissipated in the receiver plate. At anti-resonances of the receiver plate, the transmission efficiency has a minimum. When the thickness ratio $h_1/h_2$ is large, the infinite plate constrains the finite plate and the peaks tend towards the natural frequencies for a clamped edge [F–S–C–S]; when the ratio $h_1/h_2$ is small, the peaks tend towards those for a simply supported edge [F–S–S–S] with the source plate adding no further constraint.

## 5. A finite plate coupled to a semi-infinite plate of finite width

### 5.1. Model

In order to evaluate the influence of the modal behaviour of the source plate on the CLF, one can consider a finite source plate connected to a semi-infinite receiver plate, as shown in Fig. 12.

These are connected by a simply supported edge as before. For this system, it is more appropriate to simulate a 'rain-on-the-roof' type excitation as in Section 2 rather than a propagating source wave as in Sections 3 and 4. As in the investigation of two finite plates in Section 2, 400 randomly chosen excitation points are used on the finite source plate to minimize variability due to force position. For each point force, this excites vibration in many different transverse orders, $n$, across the plate width. For a given frequency, all such components have been included whose cut-on frequency is below the frequency under consideration.

The equations of motion are solved using a dynamic stiffness approach, similar to that used in Section 2. A harmonic point force is applied inside one plate. Thus the source plate is separated into two dynamic stiffness elements at the longitudinal position of the applied force. The dynamic stiffness matrix for the semi-infinite receiver plate [19] can be defined in terms of the positive-going propagating and nearfield waves at the interface. As before, the global dynamic stiffness matrix of the total system is derived by assembling the dynamic stiffness matrices of the two finite plates either side of the force location and the semi-infinite plate and applying the continuity and equilibrium conditions at the interfaces. The reduced dynamic stiffness matrix $\mathbf{K}$, for flexural motion only of order $n$, is a $5 \times 5$ frequency-dependent matrix after allowing for the simple support between the finite and semi-infinite plates. The response can be obtained from $\mathbf{K}^{-1}\mathbf{F}$ for every frequency, where $\mathbf{F}$ is the applied force vector.

The CLF can be determined from the power balance Eq. (10). As in Sections 3 and 4, no damping is included in the semi-infinite plate. Due to its infinite nature, energy is only transmitted away from the joint and the term $\omega\eta_{21}E_2^{(1)}$ representing power transmitted from plate 2 back to plate 1, is zero. Since $P_{1,diss}^{(1)} = \omega\eta_1 E_1^{(1)}$, the effective CLF for a particular finite source plate is obtained from

$$\hat{\eta}_{12} = \frac{P_{12}}{\omega E_1} = \eta_1 \frac{P_{12}}{P_{1,diss}}, \tag{26}$$

where the superscript (1) is omitted for clarity, $P_{12}$ is the power transmitted from plate 1 to plate 2 and $P_{1,diss}$ is the power dissipated by plate 1.

To evaluate the effective CLF, one needs to calculate the strain energy of the source plate $E_1$ and the power transmitted at the joint $P_{12}$. As before, the response of the source plate is integrated analytically to give an accurate measure of its strain energy [19]. The power transmitted at the interface $P_{12}$ is obtained directly from the internal moment amplitudes per unit length at the interface calculated from the elements of the dynamic stiffness matrix, and the rotation amplitudes. These are calculated for each transverse order $n$, integrated along the interface length $b$ analytically, and then summed.

### 5.2. Results

The dissipated and transmitted power for this system fluctuate due to the modal behaviour of the finite source plate, as shown in Fig. 13. In each case these are averaged over 400 forcing points. However the peaks in the two curves tend to coincide. The power transmitted becomes significantly lower than the power dissipated as frequency increases. The sharp increase in the upper curve at about 5 Hz corresponds to the cut-on frequency of the receiver plate (4.89 Hz) below which the transmitted power is zero.

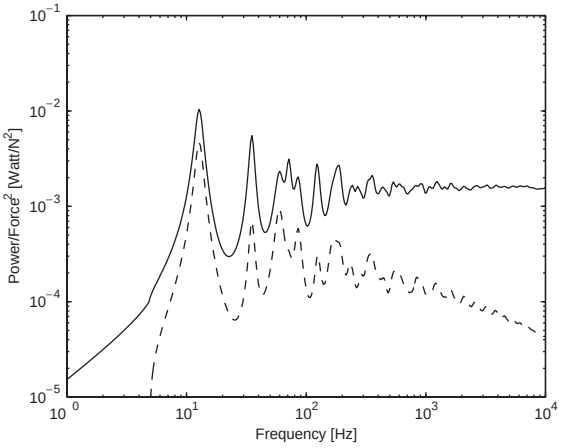


Fig. 13. The power dissipated $P_{1,diss}$ and power transmitted $P_{12}$ for a finite source plate ($h_1 = 3\,\text{mm}$, $L_1 = 0.5\,\text{m}$, $\eta_1 = 0.1$) coupled to a semi-infinite receiver plate ($h_2 = 2\,\text{mm}$, $\eta_2 = 0$) of finite width ($b = 1\,\text{m}$): ——, $P_{1,diss}$; - - - -, $P_{12}$.

The effective CLF from Eq. (26) is plotted in Fig. 14(a) accounting for transverse orders $n = 1$ up to 4. Also shown is the result for $n = 1$ to $n_{max}$, which includes all 46 transverse orders for all frequencies. This result is shown again in Fig. 14(b) in one-third octave bands. At low frequencies, the effective CLF fluctuates relative to that obtained from two semi-infinite plates, with a deviation of 7 dB at 31.5 Hz. As the number of transverse orders $n$ increases and the sum over $n_{max}$ is taken, the effective CLF converges to the CLF for two semi-infinite plates. The modal overlap of the source plate is equal to unity at about 200 Hz, above which the deviations are less than 2 dB.

As damping of the source plate is increased, the level of the peaks in the energy $E_1$ and the power transmitted $P_{12}$ decrease, as shown in Fig. 15. However damping has only a small effect on the effective CLF, as shown in Fig. 16, as similar proportional reductions occur in both the energy dissipated and the transmitted power.

### 5.3. The influence of the modal behaviour of the finite source plate

This section investigates the influence of the modal behaviour of the finite source plate on the energy transmission in terms of the effective CLF. A parameter study is performed in which the thickness ratio between the two plates is varied and the modal behaviour of the finite source plate is examined.

First, the thickness of the finite source plate is varied between 3 and 1/3 times the thickness of the semi-infinite receiver plate, which is fixed as 2 mm. The influence of the thickness of the source plate is shown in Fig. 17(a). The peaks and troughs can be related to the modal behaviour of the source plate. This will be considered in more detail below. Energy transmission starts at the cut-on frequency of the receiver plate, the thickness of which is kept the same, as indicated above, even if the cut-on frequency for the source plate is greater than this. The maximum energy transmission occurs when the two plates have the same thicknesses (see also Fig. 10).

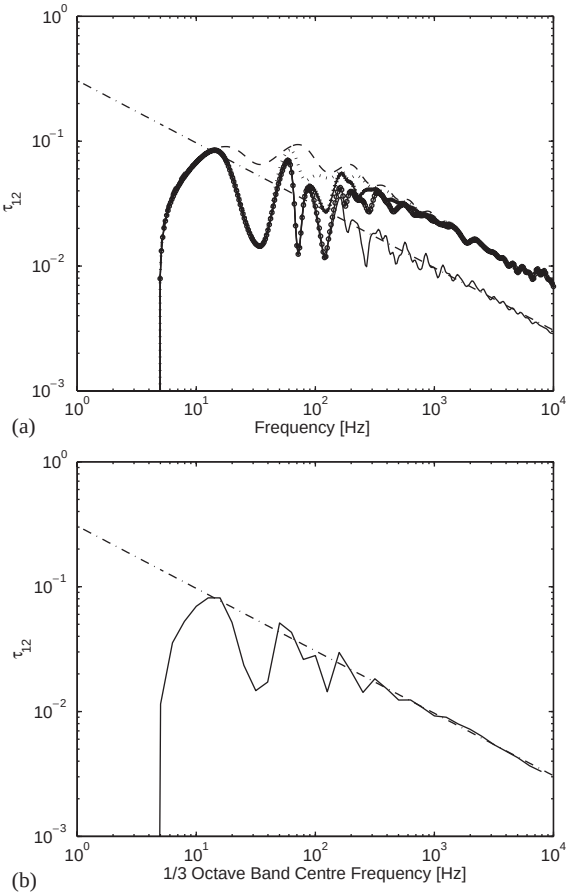


Fig. 14. Effective CLF for a finite source plate ($h_1 = 3\,\text{mm}$, $L_1 = 0.5\,\text{m}$, $\eta_1 = 0.1$) coupled to a semi-infinite receiver plate ($h_2 = 2\,\text{mm}$, $\eta_2 = 0$) of finite width ($b = 1\,\text{m}$): (a) $\eta_{12}$ versus frequency and (b) $\eta_{12}$ versus 1/3 octave frequency band: - - - -, $n = 1$; ·····, $n = 1 + 2$; −+−+−, $n = 1 + 2 + 3$; −○−, $n = 1 + 2 + 3 + 4$; ——, $n = 1$ up to 46; - · - · -, $\eta_{12\infty}$.

Next to investigate the influence on the modal behaviour due to the semi-infinite receiver plate, the thickness of the finite source plate is fixed as 3 mm and the thickness of the semi-infinite receiver plate is varied between 1/3 and 3 times this. The effective CLFs are shown in Fig. 17(b).

As before the energy transmission starts at the cut-on frequency of the semi-infinite receiver plate. The energy transmission varies as the thickness of the receiver plate is changed. The effective CLF fluctuates at low frequencies and converges to the result for the corresponding infinite plate, as shown in Fig. 14. The peaks and troughs occur at similar frequencies as the thickness of the semi-infinite receiver plate varies. These peaks can therefore be seen to depend on the modal behaviour of the finite source plate, as the thickness of that plate is fixed. The natural frequencies of an uncoupled source plate for different transverse orders, $n$ and two different boundary conditions along the edge usually joined to plate 2 have been determined. The first 12 such natural frequencies are marked in Fig. 18. Also shown is the ratio between the effective CLFs for a finite source plate ($h_1 = 3\,\text{mm}$, $L_1 = 0.5\,\text{m}$, $b = 1\,\text{m}$) coupled to a semi-infinite plate and the

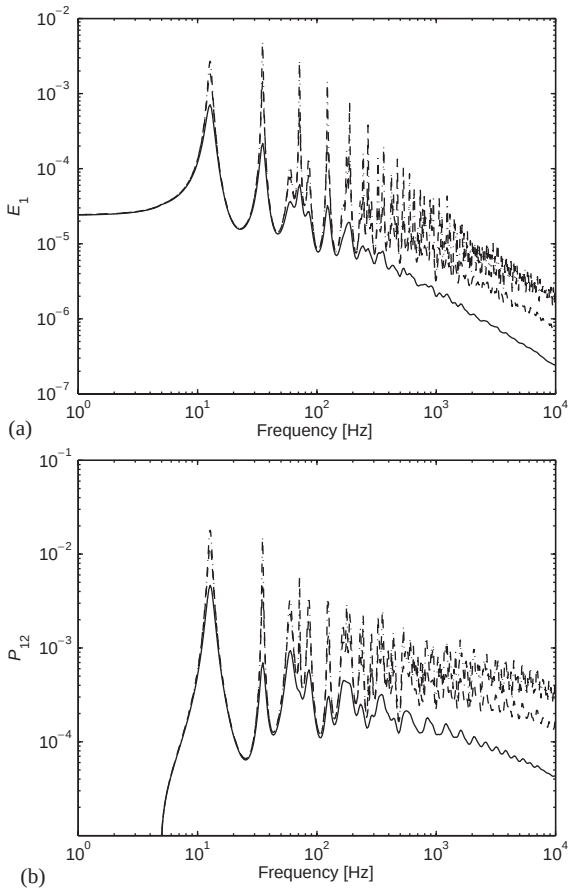


Fig. 15. The influence of damping of the finite source plate on: (a) the strain energy of the source plate $E_1$ for different DLFs and (b) the power transmitted $P_{12}$: ——, $\eta_1 = 0.1$; - - - -, $\eta_1 = 0.03$; - · - · -, $\eta_1 = 0.01$. The dimensions of the source and semi-infinite receiver plates are the same as Fig. 13.

semi-infinite results, $\hat{\eta}_{12}/\eta_{12\infty}$. The natural frequencies are shown with different symbols for each value of $n$. The upper figure gives the natural frequencies for a clamped edge and the lower figure for a simply supported edge. When $h_2 \gg h_1$, the semi-infinite receiver plate constrains the finite source plate and the peaks tend towards the natural frequencies for a clamped edge [F–S–C–S]; when $h_2 \ll h_1$, the peaks tend towards those for a simply supported edge [F–S–S–S]. However, it is also found that, whilst the first resonance corresponds to a peak in the effective CLF, the second corresponds to a dip, the third to a peak and so on.

In Fig. 19, the effective CLF for a finite source plate and semi-infinite receiver plate is compared with the CLF for two semi-infinite plates, for a diffuse field and for 4 transverse orders. Two sets of results are given, corresponding to $h_1 = 3\,\text{mm}$, $L_1 = 0.5\,\text{m}$, $b = 1\,\text{m}$, $h_2 = 2\,\text{mm}$ and $h_1 = 2\,\text{mm}$, $L_1 = 1.0\,\text{m}$, $b = 1\,\text{m}$, $h_2 = 3\,\text{mm}$. Corresponding modes of the uncoupled source plate are shown, in the first case for F–S–S–S and in the second case for F–S–C–S. The troughs in the effective CLF correspond to the first resonance for a given $n > 1$ which in turn correspond approximately to the cut-on frequency of the source plate for $n > 1$.

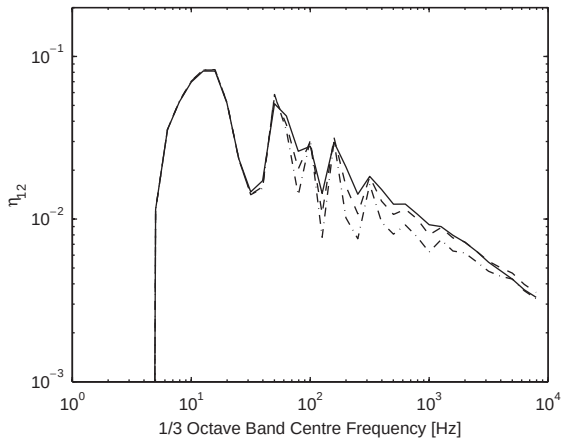


Fig. 16. The influence of damping on the effective CLF of the finite source plate ($h_1 = 3\,\text{mm}$, $L_1 = 0.5\,\text{m}$) coupled to a semi-infinite receiver plate ($h_2 = 2\,\text{mm}$, $\eta_2 = 0$) of finite width ($b = 1\,\text{m}$): ——, $\eta_1 = 0.1$; - - - -, $\eta_1 = 0.03$; - · - · -, $\eta_1 = 0.01$.

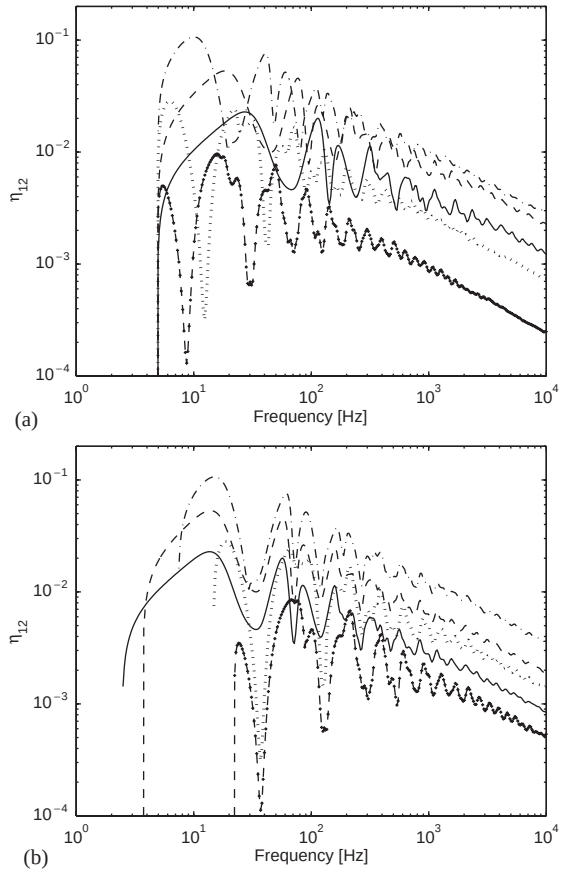


Fig. 17. The effective CLFs for transmission from a finite source plate (width $b = 1\,\text{m}$, length $L_1 = 0.5\,\text{m}$) to an infinite receiver plate for different values of $h_1/h_2$: (a) $h_2$ is fixed as 2 mm and (b) $h_1$ is fixed as 3 mm: ——, $h_1/h_2 = 3$; - - - -, $h_1/h_2 = 2$; - · - · -, $h_1/h_2 = 1$; ·····, $h_1/h_2 = 1/2$; – + – + –, $h_1/h_2 = 1/3$.

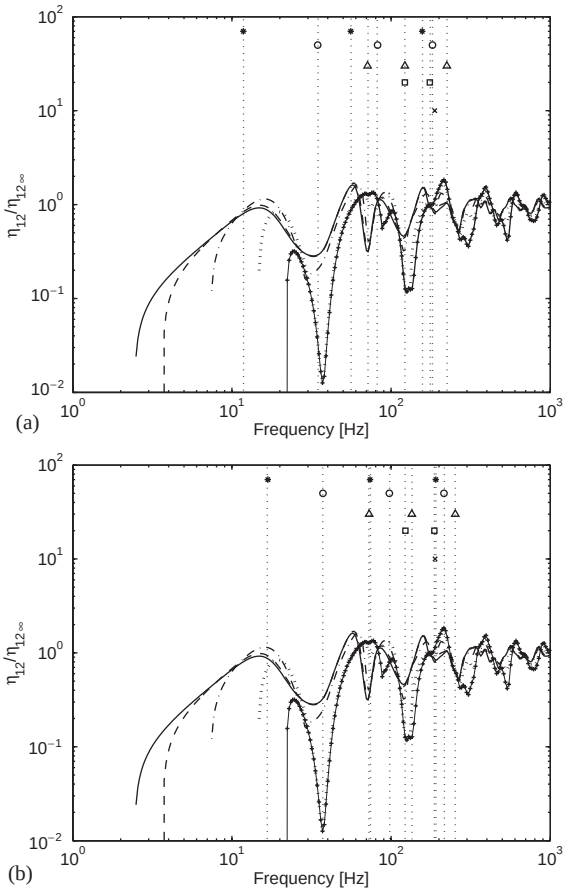


Fig. 18. The ratio between the effective CLFs for a finite plate ($L_1 = 0.5$ m, $h_1 = 3$ mm) coupled to a semi-infinite plate of finite width ($b = 1$ m) and the semi-infinite results, $\hat{\eta}_{12}/\eta_{12\infty}$: ——, $h_2 = 1$ mm; - - - -, $h_2 = 1.5$ mm; - · - · -, $h_2 = 3$ mm; ·····, $h_2 = 6$ mm; −+−+−, $h_2 = 9$ mm. The symbols denote natural frequencies of finite source plate for different boundary conditions along the edge: (a) F–S–S–S and (b) F–S–C–S, and different transverse orders $n$: $*$, $n = 1$; $\bigcirc$, $n = 2$; $\triangle$, $n = 3$; $\square$, $n = 4$; $\times$, $n = 5$. The vertical dotted lines show the natural frequency of each mode.

These results can be understood as follows. At a resonance of the finite plate, the effective angle of incidence is dominated by that corresponding to the mode. Consequently the effective CLF follows closely that for the semi-infinite plates with the corresponding order $n$. The fluctuations in the effective CLF in this case are therefore due to the predominance of particular angles of incidence, not due to the direct influence of the modal behaviour of the source plate. This explains, also, the relatively small influence of the damping of the source plate (Fig. 16).

## 6. Concluding remarks

The variability in the effective CLF, or the transmission efficiency, of finite coupled source and receiver plates due to their modal behaviour, has been examined using a systematic investigation

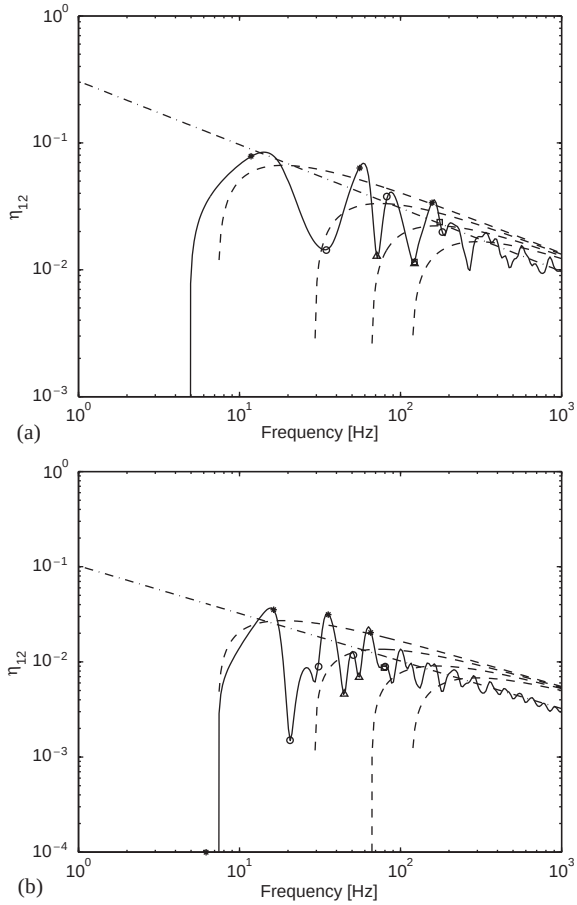


Fig. 19. Comparison of the CLFs for a finite plate coupled to a semi-infinite plate of finite width: (a) $h_1 = 3$ mm, $h_2 = 2$ mm, $L_1 = 0.5$ m, and (b) $h_1 = 2$ mm, $h_2 = 3$ mm, $L_1 = 1.0$ m: - · - · -, the CLF for two semi-infinite plates; ——, the effective CLF for a finite plate coupled to a semi-infinite plate of finite width ($b = 1$ m); - - - -, the effective CLFs obtained from Eq. (11) for two semi-infinite plates of finite width ($n = 1$, 2, 3 and 4). The symbols denote natural frequencies of finite source plate for different boundary conditions along the edge: (a) F–S–S–S and (b) F–S–C–S, and different transverse orders $n$: $*$, $n = 1$; ○, $n = 2$; △, $n = 3$; □, $n = 4$.

involving both finite width semi-infinite plates and finite plates. A combination of novel wave models and dynamic stiffness approaches has been used in the present paper, which enable a comparison between wave estimates and modal contributions.

Previously, it had been surmised [18] that the modal behaviour of the receiving subsystem had the predominant effect on the variability of the power flow, that of the source subsystem being neglected. It is shown here that the modal behaviour of both the source and receiver plates affects the energy transmission between two subsystems in the example considered. Large variability in the effective CLF was found to occur due to the modal behaviour of the receiver plate, with peaks occurring in the transmission efficiency at resonances of the receiver. The damping of the receiver plate controls the magnitude of these variations.

However, some variations in the effective CLF can also be attributed to the source subsystem characteristics, not previously considered by Craik et al. [18], whose results were based on measurements on building structures. By using simulations for a finite source plate coupled to a semi-infinite receiver plate, variations in CLF are found that are considered to be due to the predominance of particular angles of incidence at a given frequency. Damping of the source plate has been found to have a smaller influence on controlling these fluctuations than for the receiver plate resonances. Figs. 8 and 14(a) summarize these trends by comparing the effective CLFs found for a finite receiver or a finite source plate. In this case, for $\eta = 0.1$, the variation in both curves is similar and as more modes cut on the variability reduces due to the increase in modal overlap, as expected. However, as damping is reduced, the effect of the receiver plate modes will increase while that of the source plate modes will be largely unchanged [19], as seen in Figs. 9 and 16.

Finally, it may be noted that Mace found that at low modal overlap the CLFs are at a minimum for rectangular plates, compared with irregular plates [15]. This is attributed to wave coherence or localization of the global modes of the structure to one of the subsystems. It is possible that this effect may limit the extent to which the results presented here may be generalized.

## Acknowledgements

The first author gratefully acknowledges the financial support provided by the British Chevening Scholarship and Daewoo Motor Company.

## References

[1] R.H. Lyon, G. Maidanik, Power flow between linearly coupled oscillators, *Journal of the Acoustical Society of America* 34 (5) (1962) 623–639.
[2] R.H. Lyon, E. Eichler, Random vibration of connected structures, *Journal of the Acoustical Society of America* 36 (1964) 1344–1354.
[3] D.E. Newland, Calculation of power flow between coupled oscillators, *Journal of Sound and Vibration* 3 (3) (1966) 262–276.
[4] G. Borello, Prediction and control of structure borne noise transfers in vehicles using SEA, *Proceedings of Euro-Noise 98*, Munich Germany, 1998, pp. 183–188.
[5] B.M. Gibbs, C.L.S. Gilford, The use of power flow methods for the assessment of sound transmission in building structures, *Journal of Sound and Vibration* 49 (2) (1976) 267–286.
[6] P. Hynna, P. Klinge, J. Vuoksinen, Prediction of structure-borne sound transmission in large welded ship structures using statistical energy analysis, *Journal of Sound and Vibration* 180 (4) (1995) 583–607.
[7] J. Woodhouse, An introduction to statistical energy analysis of structural vibration, *Applied Acoustics* 14 (1981) 455–469.
[8] F.J. Fahy, Statistical energy analysis: an overview, in: A.J. Keane, W.G. Price (Eds.), *Statistical Energy Analysis: A Critical Overview, with Applications in Structural Dynamics*, Cambridge University Press, Cambridge, 1997, pp. 1–18 (Originally published in *Philosophical Transactions of the Royal Society of London, Series A* 346 (1994) 429–554).
[9] ESDU, *An Introduction to Statistical Energy Analysis*, Item No. 99009, ESDU International plc., London, UK, 1999.
[10] R.H. Lyon, R.G. DeJong, *Theory and Application of Statistical Energy Analysis*, 2nd Edition, Butterworth-Heinemann, Boston, 1995.
[11] F.J. Fahy, Statistical energy analysis: a wolf in sheep's clothing? *Proceedings of Internoise* 93, 1993, pp. 13–67.

[12] F.J. Fahy, A.D. Mohammed, A study of uncertainty in application of SEA to coupled beam and plate systems, Part I: computational experiments, *Journal of Sound and Vibration* 158 (1) (1992) 45–67.
[13] L. Cremer, M. Heckl, E.E. Ungar, *Structure-borne Sound*, 2nd Editon, Springer, New York, 1988.
[14] B.R. Mace, The statistical energy analysis of two continuous one-dimensional subsystems, *Journal of Sound and Vibration* 166 (3) (1993) 429–461.
[15] B.R. Mace, J. Rosenberg, The SEA of two coupled plates: an investigation into the effects of system irregularity, *Journal of Sound and Vibration* 212 (1999) 395–415.
[16] E.C.N. Wester, B.R. Mace, Statistical energy analysis of two edge-coupled rectangular plates: ensemble averages, *Journal of Sound and Vibration* 193 (4) (1996) 793–822.
[17] F.F. Yap, J. Woodhouse, Investigation of damping effects on statistical energy analysis of coupled structures, *Journal of Sound and Vibration* 197 (1996) 351–371.
[18] R.J.M. Craik, J.A. Steel, D.I. Evans, Statistical energy analysis of structure-borne sound transmission at low frequencies, *Journal of Sound and Vibration* 144 (1) (1991) 95–107.
[19] W.S. Park, The Sources of Variability in the Statistical Energy Analysis of Two Rectangular Plates, Ph.D. Thesis, University of Southampton, Southampton, UK, 1999.
[20] R.S. Langley, Application of the dynamic stiffness method to the free and forced vibrations of aircraft panels, *Journal of Sound and Vibration* 135 (2) (1989) 319–331.
[21] D.A. Bies, S. Hamid, In situ determination of loss and CLFs by the power injection method, *Journal of Sound and Vibration* 70 (1980) 187–204.
[22] R.G. DeJong, An approach to the statistical energy analysis of strongly coupled systems, in: F.J. Fahy, W.G. Price (Eds.), *Proceedings of IUTAM Symposium on Statistical Energy Analysis*, Kluwer Academic Publishers, Dordrecht, 1999, pp. 71–82.